Design Considerations for a GBT Q-Band Array Receiver

E. Wollack and S. Srikanth
NRAO, Charlottesville, VA
April 9, 1995

1. Introduction

We plan to construct a prototype module of the GBT Q-band 40–50 GHz array receiver. Four L/R-polarization modules forming an eight-channel receiver is envisioned. In this memo the receiver layout, array geometry, and cryogenic package are outlined. Critical components are indicated, as well as anticipated problem areas and trade-offs required in realization of the array.

2. System Considerations

From a spectroscopist's perspective, the ideal frequency coverage for the array would encompass the 42.5 GHz SiO to the 51.8 GHz C_3H_2 lines (Wootten 1991). The rapidly increasing O_2 atmospheric contribution would tend to favor the lower end of such a band for continuum observations. Polarizer and low-noise amplifier designs for 40–50 GHz developed for the VLBA are available in WR22 (33–50 GHz for single mode $TE_{1,0}$). Employing these components would result in acceptable system performance above 50 GHz. Given the existing resources, this provides the most cost-effective solution.

The bandwidth limiting component in the front-end will be the cryogenic circulators [1]. A trade-off between bandwidth and isolation/VSWR is made in realizing the structure. For a 10 GHz bandwidth, an isolation of ~ 20 dB and an insertion loss of -0.4 dB are obtained in practice at ~ 20 K. It is recommended that the circulators are specified from 41–50 GHz, and a gradual deterioration in isolation is accepted near the band edges.

[1] To maintain the independence of the R/L-channels, a circulator is required. If linear polarization were employed, the isolator between the amplifier and the orthomode could be dropped in an off-axis system. The degradation in system performance associated with this isolator is deemed acceptable in order to provide VLBI compatibility.

A low-level noise source will be injected after the polarizer to monitor the receiver calibration stability. At this stage no provision for a front-end phase-calibration signal is provided. System phase calibration from the first IF to the back-end could be implemented with existing hardware at a later date.

For spectral line work, HEMT gain instability will not be a concern due to the narrow bandwidth. Refer to discussion in Wollack (1995) . The prototype module will serve as a test platform to address this problem for broadband continuum observations. In addition to increasing the system noise, the presence of low frequency fluctuations complicates spectral determination for low signal-to-noise continuum observations. In a total power system modulated at 10 Hz with existing HEMT devices, a rf bandwidth of 0.8 GHz can be supported with a 10% penalty in noise (see Appendix A.). Ultimately, a ~ 4 GHz instantaneous bandwidth for continuum observations is desirable at Q-band. To support this bandwidth, an effective chop rate > 500 Hz is required. We note, however, given the magnitude of this effect, spectral line performance should not be compromised in achieving this goal.

See Table 1 for a summary of component, signal processing, and system level approaches to improve stability. In general, easily implemented solutions have little effect on improving the rf bandwidth. Clearly the best method to eliminate this problem is to increase the effective switching rate above that practical with a mechanical beam switch. This modulator should be as far forward in the front-end as practical—in an ideal situation, position switching the telescope would be sufficient. A cryogenic Dicke switch would provide a more than adequate switch rate; however, the circulator bandwidth considerations discussed above might prove problematic [2]. A broadband analog correlator or a double-pole-double-throw transfer switch in the IF provide reasonable alternative engineering solutions to be investigated in achieving this goal.

3. Cryogenic Package

See Figure 1 for a block diagram of the dewar package. Commercial WR22 noise sources are available with a +21 dB excess noise ratio. This is adequate to provide a ~ 10 K injected calibration signal at the LNA input. Cooling the mixer and first IF amp shaves ~ 20 K off the system noise near the band edges. In addition, cooling the mixer lowers the required rf

[2] Amplitude cross-coupling in the isolator will cause a residual image beam response at the 10% level—this is considered unacceptable and would prevent an affordable double Dicke switch receiver implementation. Such devices provide a viable solution for $< 10\%$ fractional system bandwidths and cost about \$5k each (Electromagnetic Sciences, Inc.).

gain and the input power level to the mixer. This is desirable from both the standpoint of gain stability improvement and spurious mixer response reduction. For the estimated system noise temperature, see Table 2. Without some form of gain equalization, it is unlikely that the ± 5 dB GBT back-end flatness specification will be met over the entire rf band.

Estimates of the thermal load to the refrigerator are provided in Table 3. A CTI 1050 head will provide 65 W cooling power to the 77 K stage and 7 W to the 15 K stage. Cooling the corrugated feed will reduce the system temperature by ~ 6 K. For this reason, it is believed that the added complication of the relatively large vacuum window is desirable. Initial calculations indicate that a seven-feed hex window may prove difficult to implement. A four-feed, dual-polarization arrangement is preferred from a thermal loading and mechanical design standpoint. A prototype window will be fabricated to determine the most reliable configuration.

4. Frequency Conversion

The receiver must be compatible with the GBT back-end currently under construction. This 8-channel IF is specified to operate from 1 to 8 GHz. Two local oscillators operating from 0.3—20 GHz are available in the GBT receiver turret. See Figure 2 for the RF down conversion scheme. LO1 is provided by a +10 dBm active 4× multiplier (supplied by DBS). If four units are employed in the array, the balanced mixers will need to be biased ($P_{\mathrm{LO1}} \cong +5$ dBm/mixer). With this scheme, a 7 GHz image-free instantaneous bandwidth is present in the frequency range of 40 to 49 GHz. For example, tuning the LO1 to 41 GHz will present 42–49 GHz to the GBT back-end. [3]

Tuning LO1 above 41 GHz will result in the lower portion of the rf band corrupting the lower part of the GBT IF band. Noting the maximum supported image-free bandwidth, 4 GHz, is larger than the current spectrometer instantaneous bandwidth, 0.8 GHz, this is not seen as a potential problem for spectral line work in the near future. For continuum observations, subdivision of the IF into 1–4.5 GHz and 4.5–8 GHz bands (or finer) would be desirable. With this conversion scheme, the lowest spurious mixer intermodulation response is $2\,\mathrm{LO1} - 2\,\mathrm{RF}$. Given the balanced mixer design, by symmetry, this response should be small. The manufacturer estimates this response to be less than -90 dBc.

We note in this band only 42.5–43.5 GHz (SiO line) and 48.94–49.04 GHz (CS line) are

[3] A high/low-side LO scheme would eliminate the image problem; however, a ~ 2 dB increase in mixer conversion lost and a reduction in flatness would result.

officially allocated for primary radio astronomy usage (ITU 1990). The remainder of the band should be fairly clear of man-made interference due to the current void of systems in this frequency range. However, the Milstar satellite secure communication channel at 44 GHz and other proposed systems may have to be contended with by the time the GBT is in use.

5. Array Feeds and Optics

Spillover contribution is a small fraction of the system temperature at Q-band; hence, sensitivity and aperture efficiency peak around the same feed taper. A feed taper of -12 dB at the edge of the subreflector where the aperture efficiency peaks is chosen. A linear taper horn would have an outside diameter (OD) of 3.125" and when arranged in a 2×2 array would give beams in the sky separated by 4.7 and 6.1 half power beam widths (HPBW) at 40 and 52 GHz, respectively. A profile horn with the same taper as above would have an OD of 2.080", rendering a more compact array and with beams separated by 3.1 and 4.0 HPBW's at the band edges. However, aperture efficiency is lower by about 4% with the profile horn.

The settle time of the telescope will not allow rapid position switching of the telescope—the primary must slowly track objects (RSI 1993, Gawronski and Parvin 1994). A set of tertiary reflectors, one of them a chopping mirror, is envisioned for atmospheric noise suppression, fast pointing corrections, and scanning of the array during mapping. We have also investigated the following:

- Differencing fixed position beam spacings
- Rotating chopper with variable beam spacing

and note neither scheme allows implementation of fast pointing corrections. The chopping reflector can be either flat or curved while the other reflector is flat. A chopping flat has the advantage of being relatively inexpensive, light-weight, and possessing both broad frequency bandwidth and angular response. A curved or shaped focusing element will typically have a smaller maximum scan angle and is usually suitable for a single beam. The long transition times and blanking generally associated with quasi-optical modulators can be avoided by the use of a continuous scan strategy. Mechanical choppers in general have the disadvantages of providing a relatively slow modulation rate, being somewhat mechanically complex, and having synchronously modulated emission and spillover which cause a non-zero instrumental offset in lock-in data.

For a mechanically driven plate, the maximum chop frequency scales as, $f_{\rm chop} \propto (T/\theta_{\rm t} I)^{1/2} \propto (T/\theta_{\rm t} r^5)^{1/2}$, where T is the available torque, $\theta_{\rm t}$ is the beam throw angle, I is the chopper moment of inertia, and r is the chopping plate radius. In practice, the maximum available torque is essentially a constant determined by the chopper drive technology employed. A premium is placed upon reduced size and weight in achieving a high chop rate. The plate should chop at ~ 10 Hz to provide atmospheric suppression. Scaling previous chopper designs indicates this goal can be achieved. The lowest rf operating frequency of the tertiary drives both the cost and size of the nutator. Increasing the chopper size to support an array at half the rf frequency would reduce the maximum chopper frequency by a factor greater than 4. Traditional chopping plate designs with plate throw angles greater than $\delta\theta_{\rm c} \sim \pm 5°$ are somewhat difficult to implement. This places a practical limitation on the sky throw angle, $\theta_{\rm t} \cong 2\delta\theta_{\rm chopper}/M \sim \pm 1.5'$, where, $M \simeq 400$, is the magnification in the chopper plane.

Nominally the array will be centered on the optical boresight axis to minimize beam efficiency loss with throw. Due to the choice L/R-polarization, the beams will have beam squint in AZ. For optimal atmospheric cancellation, the array beams should have as uniform shape, spillover, and deterioration with throw as possible.

The pair of flat tertiary reflectors proposed will scan the beams in azimuth. Figure 3 shows the layout of the reflectors in the symmetric plane of the telescope. The center of the feed array is offset along the symmetric plane from the secondary focus. Reflector 'A' is on the array axis while reflector 'B' is located above the secondary focus. By chopping reflector 'A' about an axis along the boresight of the array, the telescope beam is made to scan in azimuth only. For a single feed, reflector 'A' could be curved, resulting in a smaller reflector 'B', by about 20%. The locations and orientations of the two reflectors have been chosen to optimize size and minimize blockage effects.

Reflector 'A' is elliptical in cross-section (10.7" $\times$ 9.5"), while reflector 'B' is a rectangle of 30.3" $\times$ 36.0". Illumination is about -24 dB at the edge of the two reflectors at 46 GHz and -19 dB at 40 GHz. The critical parameter in the optics design is the horizontal distance between the center of the two reflectors. The dewar is envisioned to have a radius of 6" around the array center. The on-axis ray from feed '2' intersects reflector 'B' at a distance of 19.2" from the center of the array along the turret plane. When the dewar is installed in one of the 36" diameter holes on the turret with the center of the array at a distance of 12" from the center of the hole, the effective phase centers of the reflected beams off reflector 'B' (feed pairs '1-2' and '3-4') would be at distances of 5.1" and 7.2" from the secondary focus. Refocusing the subreflector is not deemed necessary with the above offsets; however, carrying out this optimization will change the beam locations slightly. Table 4 gives aperture efficiency, HPBW, and beam spacing for the array without and with the tertiary reflectors.

For the case without tertiary, the array is centered about the secondary focus, while for the second case the phase centers have been translated along the focal plane from the focus. The drop in efficiency is due to loss through the tertiary (about 1%) and phase loss due to the phase centers being not at the focus. The HPBW does not change for the two cases; however, the axial ratio deteriorates from 1.0 to 1.02. Table 5 shows the beam locations for the above two cases. When the tertiary is chopped through 4 degrees, the beam is scanned in the sky by 73 arcsecs with a drop in efficiency of 0.7%.

With the tertiary reflectors, the phase centers of the feeds get translated downward by 20.9"; hence, the dewar should be located with the aperture of the feeds 22.8" above the turret plane. In order to track a source in the parallactic angle with the array, the dewar will be mounted on a rotating ring which will be installed inside the turret hole offset to one side. The tertiary reflectors will be installed independent of the dewar mount. The tertiary system proposed here is optimized for Q-band, but it could be usable with a single beam at > 22 GHz. The design is constrained by available space in a turret hole.

6. Recommended Configuration

An estimate of the total receiver component cost per module is provided in Table 6. A 7 GHz IF is chosen for compatibility with the GBT back-end currently under construction. Initially, a 0.8 GHz continuum bandwidth will be supported. Investigations will be undertaken to allow utilization of a $\sim$ 4 GHz rf bandwidth. A two-polarization, four-element grid is preferred upon considering chopper size and thermal loading. The optics concept presented here is optimized for Q-band operation with a chopper. The feasibility of a removable general purpose tertiary design for operation > 18 GHz will be investigated.

A. Instrumental Stability and Noise Correlation Estimates

A power law dependence in frequency for the HEMT fluctuation spectral density,

$$\delta g^2(f) \equiv \delta g^2 / \left(f/1\mathrm{Hz}\right)^{\alpha} \tag{A1}$$

and $\alpha \cong 1$ is assumed. A Q-band LNA gain stability of $\delta g^2 \cong 5\,\mathrm{GHz}^{-1}$ has been achieved in the laboratory with a $\sim 1\,\mathrm{K}$ increase in T_{N} over that achievable with a minimum noise bias. Assuming a chop rate of $f_{\mathrm{chop}} = 10\,\mathrm{Hz}$ and a maximum desired increase in system noise of $\epsilon = 0.1$, we find,

$$f_{\mathrm{chop}} = \left(\frac{3}{2\epsilon + \epsilon^2} \frac{\Delta\nu_{\mathrm{rf}} \delta g^2}{6}\right)^{1/\alpha} [\mathrm{Hz}], \tag{A2}$$

a rf bandwidth of $\Delta\nu_{\mathrm{rf}} \cong 0.8\,\mathrm{GHz}$ can be supported.

If two 0.8 GHz bands are formed from a common amplifier, an instrumental correlation between the two data channels,

$$\rho_{ii'} \cong \frac{\delta g^2(f)}{2/\Delta\nu_{\mathrm{rf}} + \delta g^2(f)} \sim 0.2, \tag{A3}$$

will be present. The instrumental correlation between differing array elements, $\rho_{ij} \sim 0$, is set by the optical isolation. In practice, the observed ρ_{ij} will be dominated by residual atmospheric induced correlations in the lock-in data (see Appendix B.).

Assuming $T_{\mathrm{sys}} \cong 40\,\mathrm{K}$, $\Delta\nu_{\mathrm{rf}} = 4\,\mathrm{GHz}$ and a 10 Hz lock-in with this level of instability, the noise equivalent temperature, NET, in each receiver channel will be,

$$\mathrm{NET} = T_{\mathrm{sys}} \left(1/\Delta\nu_{\mathrm{rf}} + \delta g^2(f)/2\right)^{1/2} \cong 0.9\,\mathrm{mK}\,\mathrm{sec}^{1/2}, \tag{A4}$$

or a noise level which is factor of 1.4 times greater than expected from an ideal continuum receiver with $\delta g^2(f) \equiv 0$.

If an amplifier's 4 GHz rf bandwidth is divided into two equal channels, a $> 500\,\mathrm{Hz}$ chop rate is required to reduce the instrumental correlation to an insignificant level, $\rho_{ii'} \sim 0.01$. For this reason, a mechanical chopper is not seen as a viable solution to the receiver stabilization demands. In making these estimates, we implicitly assume that *all* of the observed low frequency fluctuations originate from the LNA. In practice, due to the behavior of HEMT devices with temperature and the low noise bias, this presents the dominate contribution to $\delta g^2(f)$.

B. Atmospheric Induced Correlations

When the beam throw is greater than the outer turbulence scale, control of the atmospheric noise with the chopper will be compromised. Assuming during periods of 'good' seeing an outer turbulence scale, $L_{\rm o} \sim 10 - 100\,{\rm m}$ (Church 1995) and an atmospheric emission scale height, $h \sim 3\,{\rm km}$; the beam throw, $\theta_{\rm t}$, should be limited to

$$\theta_{\rm t} < L_0/h \sim 10', \tag{B5}$$

for an instantaneous beam transition. The fractional two-point beam overlap is given by,

$$Q \simeq \frac{1}{\pi}\left[2\cos^{-1}\left(\theta_{\rm t}\frac{h}{D}\right) - \sin\left(2\cos^{-1}\left(\theta_{\rm t}\frac{h}{D}\right)\right)\right] \tag{B6}$$

where $D = 100\,{\rm m}$ is the telescope aperture diameter (Emerson *et al.* 1979). At a $\theta_{\rm t} = \pm 5\theta_{\rm HPBW} \simeq \pm 1.3'$ throw, we find $Q \cong 0.98$, or a few percent atmospheric correlation level might be expected. The residual instrumental correlations should be small compared to this level for optimal array performance. Assuming an average near field wind speed of $v_{\rm h} \sim 5{\rm m\,sec^{-1}}$, we find $f_{\rm chop} \gg v_{\rm h}/L_{\rm o} \sim 0.5\,{\rm Hz}$ is required to provide effective cancelation. Near field emission regions large compared to the telescope diameter are suppressed to lowest order by the beam switch regardless of the beam area overlap. These structures will drift through the beam on time scales greater than $D/v_{\rm h} \sim 20\,{\rm sec}$.

If the effective beam size is substantially increased by surface errors, telescope vibrational motion, or under-filling the aperture, the required beam throw will increase, as will the atmospheric induced correlations. This will have the net effect of increasing the allowed magnitude of instrumental-induced correlations from the value assumed in Appendix A.

References

Blum, E. 1959, *Ann. Astrophys.*, **22(2)**, 140

Church, S. 1995, *Mon. Not. R. Astron. Soc.*, **272**, 551

Colvin, R. 1961, *A Study of Radio Astronomy Receivers*, Technical Report Radio Sci. Lab. Sci. Rept. 18, Stanford Electron. Lab., Stanford, Calif.

Emerson, D., Klein, U., and Haslam, C. 1979, *Astron. Astrophys.*, **76**, 92

Gawronski, W. and Parvin, B. 1994, *Dynamic Pointing Modeling and Simulations of the 100M Green Bank Telescope (I–III)*, Technical report, JPL

Graham, M. 1958, *Proc. IRE*, **46**, 1966

ITU 1990, *Radio Regulations*, Vol. 1, General Secretariat, Geneva

Jarosik, N., Page, L., Wilkinson, D., and Wollack, E. 1993, *'Measurements of the Low Frequency Noise Properties of a 30 GHz High-Electron-Mobility-Transistor Amplifier*, Technical Report 95955, Princeton University

Orhaug, T. and Waltman, W. 1962, *Publ. Natl. Radio Astron. Obs.*, **1**, 179

Predmore, C., Erickson, N., Huguenin, G., and Goldsmith, P. 1985, *IEEE Trans. Microwave Methods and Tech.*, **MMT-33(1)**, 44

RSI 1993, *Final Analysis Report for the Green Bank Telescope Control System*, Technical Report FCM2N165.WP5, RSI, PCD Program 1010, pp. 75–82

Ryle, M. 1952, *Proc. R. Soc. London, Ser. A*, **211**, 351

Weinreb, S. 1964, *Proc. 1964 Internat'l Conf. on Microwaves, Circuit Theory, and Information Theory (summaries of papers)*, pp 95–96

Wollack, E. 1995, *High-Electron-Mobility-Transitor Gain Stability and its Design Implications for Wide Band Millimeter Receivers*, preprint

Wootten, A. 1991, *Long Millimeter-Wave Science with the GBT*, GBT Memo 109

Wornell, G. 1993, *Proc. IEEE*, **81(10)**, 1428

Table 1

Summary of HEMT Receiver Stabilization Techniques

	Complexity	Flexibility	$\Delta\nu_{\mathrm{rf}}$	Noise
High Stability HEMT Bias	+	+	−	−
Pulsed HEMT LED Mode	+	+	−	+
Regress HEMT I_{ds} (Jarosik *et al.* 1993)	+	+	−	+
Optimal Whitening Filter (Wornell 1993)	−	+	−	+
Cryogenic Ferrite Dicke-Switch	+	−	+	−
Quasi-Optical Position-Switch	−	+	−	+
Noise Source Stabilization (Weinreb 1964)	−	+	−	−
Pilot Signal Stabilization (Colvin 1961)	−	−	+	−
Gain-Switch Receiver (Orhaug and Waltman 1962)	−	−	+	−
Transfer-Switch Receiver (Graham 1958)	−	−	+	+
Phase-Switch Receiver (Ryle 1952)	−	−	+	+
Comparison Receiver (Predmore *et al.* 1985)	−	−	+	+
Correlation Receiver (Blum 1959)	−	−	+	+

In the table a designation '+' indicates the following for a given stabilization technique: 'complexity'—the technique is easy to implement, 'flexibility'—the usage of system is not hampered, '$\Delta\nu_{\mathrm{rf}}$'—the bandwidth improvement is large, and 'Noise'—the stabilization improvement does not inherently increase the system temperature.

Table 2

GBT 40–50 GHz, 8-Channel Receiver: System Temperature

Component	Gain/Loss [dB]	T_{amb} [K]	T_{N} [K]	T_{sys} [K]
CMB	–	2	2	2
Atmosphere	-0.2—-3	~ 250	~ 10—130	~ 10—130
Antenna Spill	–	10—300	~ 2	~ 2
Vacuum Window	-0.05	77—300	~ 3	~ 3
Feed	-0.1	15	0.3	0.3
Polarizer/OMT	-0.2	15	0.7	0.7
Cryo Isolator	-0.4	15	1.3	1.3
Cryo HEMT Amp	$+30 \pm 3$	15	15	15
Cryo Isolator	-0.4	15	1.3	–
Cryo Mixer	-8 ± 2	15	~ 500	~ 0.5
Cooled Isolator	-0.4	77	1.3	–
Cooled IF1 Amp	$+35 \pm 1$	77	20	0.2
SS Coax	-0.8	77—300	~ 40	–
Total	$+54 \pm 6$			35—160

Table 3

GBT 40–50 GHz, 8-Channel Receiver: Estimated Thermal Load

Thermal Source	Number	Heat Load	Heat Load
		300 → 77 K	77 → 15 K
	[–]	[Watts]	[Watts]
Radiation ($\varepsilon_{\rm Al} \sim 0.1$, $A \cong 8 \times 10^3 {\rm cm}^2$)	1	20	0.1
Thermal Stand-offs	3	3	0.6
Window (Spacer Conduction)	1	1.2	–
Window (IR Block, $A \cong 250 {\rm cm}^2$)	4×1	11	2
Wiring (#32 Brass)	4×32	1.6	0.3
HEMT DC Bias (2V, 50mA)	4×2	–	0.8
Mixer DC Bias (3V, 4mA)	4×2	–	0.1
IF1 DC Bias (3V, 70mA)	4×2	1.7	–
Waveguide, SS, Au Plate	4×2	1.4	0.3
Waveguide, SS	4×1	0.2	0.1
Coax, SS	4×2	0.3	0.1
Total		40	4.4

Table 4

GBT 40–50 GHz, 8-Channel Receiver: Estimated Beam Parameters

ν	Array	$\eta_{\rm apt}$(Boresight)	$\eta_{\rm apt}$(Tertiary)	$\theta_{\rm HPBW}$	$\left\langle \Delta\theta^{\rm beam}_{\rm spacing} \right\rangle$
[GHz]	Position	[–]	[–]	[arcsec]	[$\theta_{\rm HPBW}$]
40	$1-4$			18.4	3.1
46	$1,2$	0.561	0.551	16.0	3.5
46	$3,4$	0.563	0.557	16.1	3.6
50	$1-4$			14.7	3.9

Table 5

GBT 40–50 GHz, 8-Channel Receiver: Nominal Beam Locations

Array Position	$\theta_{\rm AZ}$(Boresight) [arcsec]	$\theta_{\rm EL}$(Boresight) [arcsec]	$\theta_{\rm AZ}$(Tertiary) [arcsec]	$\theta_{\rm EL}$(Tertiary) [arcsec]
1 L/R	−28.7	+28.8	−28.6	+198.
2 L/R	+28.7	+28.8	+28.6	+198.
3 L/R	−28.6	−28.5	−28.6	+141.
4 L/R	+28.6	−28.5	+28.6	+141.

Table 6

GBT 40–50 GHz, 8-Channel Receiver: Estimated Cost

Item	Number/Module [–]	Item Cost [$]	Cost/Module [$]
Cryo Head (1050 CP)	1/4	8200	2050
Dewar Materials	1/4	1000	250
Window	1/4	–	–
Temperature Sensor	2/4	200	100
Vacuum Sensor	2/4	60	30
Feed	1	–	–
Polarizer/OMT	1	3250	3250
Noise Source	2/4	2200	1100
Cal Splitter	6/4	500	750
Cryo Isolator	4	1100	4400
Cryo Amp Materials	2	1000	2000
Cryo Mixer	2	3200	6400
LO1 Active 4× Multiplier	1	7000	7000
LO1 Drive BPF	1	600	600
LO1 Splitter	6/4	500	750
Transfer Switch	1	–	–
Cooled IF1 Amp	2	3700	7400
IF1 Amp	2	1000	2000
WR22 Loads	28/4	110	770
Coax Loads	2	30	60
Coax Pads	2	50	100
Misc. WG/Flanges	–	500	500
Bias Connectors	5	24	120
Bias Cards	5	100	500
Misc. Electronic	–	500	500
Module Total			40,630
Receiver Total			162,520

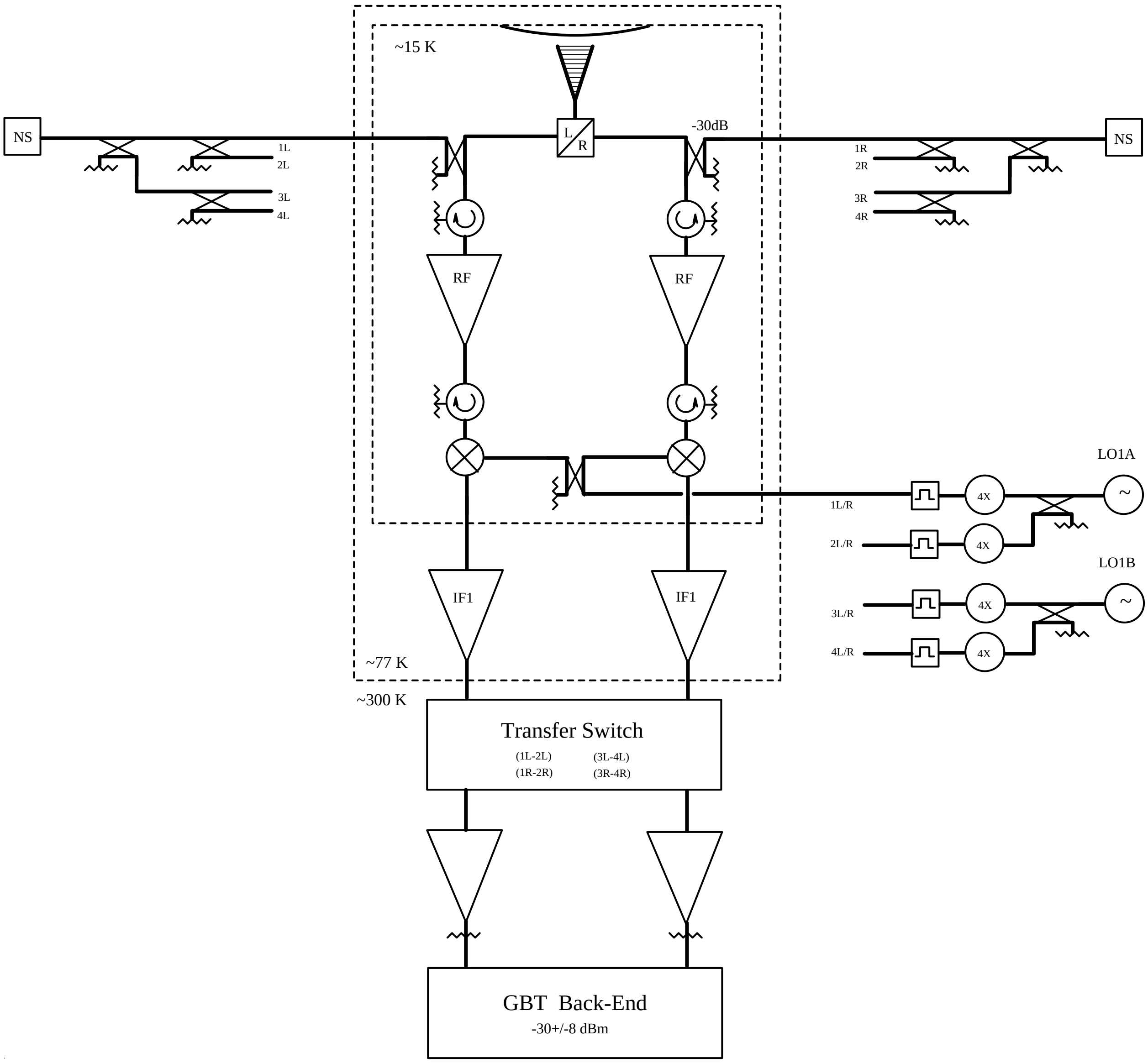

Figure 1. GBT 40–50 GHz, 8-Channel Receiver: Block Diagram

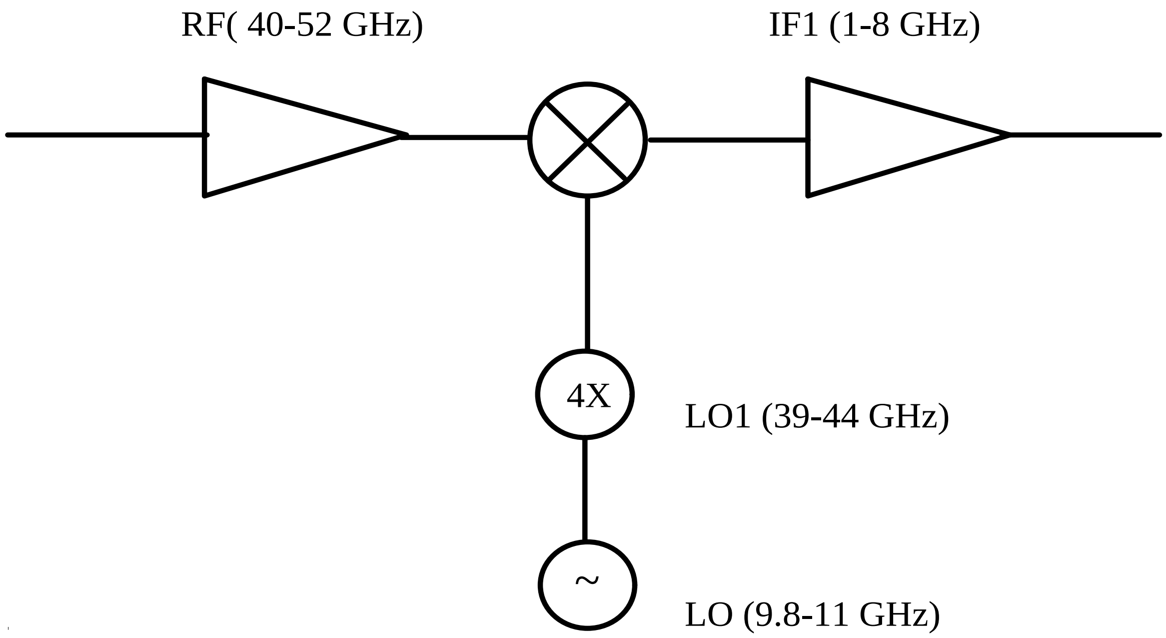

Figure 2. GBT 40–50 GHz, 8-Channel Receiver: Frequency Conversion

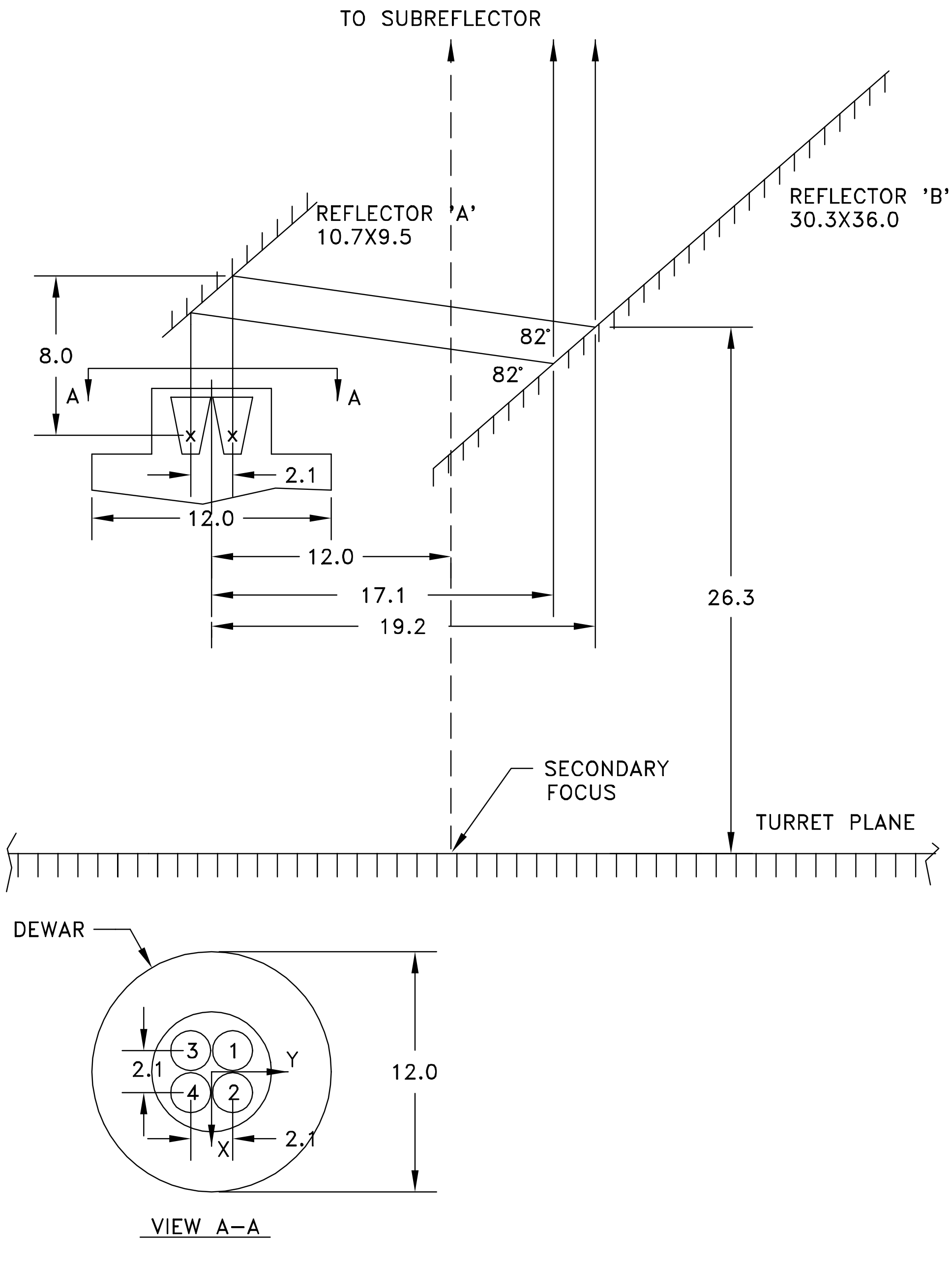

Figure 3. GBT 40–50 GHz, 8-Channel Receiver: Optics Mechanical Layout